

# Novel hyper-viscoelastic approach to modelling elastomer mechanic behaviour with relaxation spectrum



Penghao Pei <sup>a,b,c</sup>, Yueming Du <sup>a,b,c</sup>, Yinggang Miao <sup>a,b,c,\*,\*\*</sup>, Tao Suo <sup>a,b,c,\*</sup>

<sup>a</sup> School of Aeronautics, Northwestern Polytechnical University, Xi'an, 710072, PR China

<sup>b</sup> Shaanxi Key Laboratory of Impact Dynamics and Engineering Application, Northwestern Polytechnical University, Xi'an, 710072, PR China

<sup>c</sup> Joint International Research Center of Impact Dynamics and Its Engineering Application, Northwestern Polytechnical University, Xi'an, 710072, PR China

## ARTICLE INFO

### Keywords:

Hyper-viscoelastic model  
Relaxation spectrum  
Elastomer  
Strain rates

## ABSTRACT

Elastomers, such as polyurethane, exhibit hyperelastic behaviour and distinct rate dependence under a wide range of strain rates. Herein, a methodology for developing a hyper-viscoelastic constitutive model for succinctly characterising the mechanical behaviour of polyurethane under large deformations and a wide range of strain rates is proposed. The model is constructed using a long-term hyperelastic formulation combined with a rate-dependent viscoelastic model. This model is based on internal state variables and a finite strain formulation. A polyurethane elastomer was used as a sample to develop this model, by way of testing wide strain-rate mechanical behaviour ( $0.001\text{--}5000\text{s}^{-1}$ ) and viscoelastic behaviour. The viscoelastic behaviour was obtained using the equivalent time-temperature superposition relation. A parameter-fitting algorithm was adopted to separate the long-term behaviour from the viscoelastic behaviour. The long-term behaviour was modelled using a Mooney–Rivlin hyperelastic model, and its parameters were identified using the least-squares method. The time-dependent viscous effect calculated using the Prony series-based model was approximately determined based on the continuous relaxation spectrum. The characterisation capacity was confirmed through a thorough comparison with experimental curves. This model can be extended to other elastomers, even under tension, without any specific limitations of the internal components.

## 1. Introduction

Elastomers, such as thermoplastic polyurethane (TPU), exhibit a versatile combination of mechanical properties that are desirable for ballistic applications such as laminated glass windscreens, helmets, and transparent armour [1–4]. The involved structures are designed to prevent severe harm from high-velocity impacts, which requires the polyurethane elastomers to have special characteristics, such as high resilience, tensile strength, and shock absorption. In such applications, materials are expected to carry loads over extremely short periods. As unique polymers, elastomer materials have complex behaviour, including nonlinear elasticity at large deformation [5], and distinct strain rate effect [6,7] under various strain rate loadings. Thus, a thorough understanding of the mechanical behaviour of polyurethane elastomers is essential for designing the safety and evaluating the protective performance of structures against impact. It is also crucial for the constitutive characterisation required for the numerical simulation of structures.

The mechanical performance of various polyurethane elastomers under a wide range of strain rates has been investigated for many decades. Yi et al. [8] conducted a study on the mechanical properties of thermoplastic polyurethane elastomers, specifically focusing on their response to both quasi-static and dynamic loading conditions. Sarva et al. [9] conducted uniaxial compression experiments to study the stress–strain behaviour of polyurethane elastomers at strain rates ranging from 0.001 to  $5000\text{ s}^{-1}$ . Liao et al. [10] and Fan et al. [11] studied the tensile stress–strain behaviour of polyurethane, specifically examining its response under quasi-static to intermediate strain rate loading. These investigations revealed that polyurethane elastomers exhibit highly non-linear stress–strain behaviour at large strains and distinct strain rate effects: the rubber-like behaviour was exhibited at low rates and the leather-like behaviour transitioned at high rates.

To describe the rate-dependent behaviour of polyurethane, Qi et al. [5] and Cho et al. [12] proposed micromechanical models with a multiplicative decomposition of the deformation gradient and thermally

\* Corresponding author. School of Aeronautics, Northwestern Polytechnical University, Xi'an, 710072, PR China.

\*\* Corresponding author. School of Aeronautics, Northwestern Polytechnical University, Xi'an, 710072, PR China.

E-mail addresses: [ygmiao@nwpu.edu.cn](mailto:ygmiao@nwpu.edu.cn) (Y. Miao), [suotao@nwpu.edu.cn](mailto:suotao@nwpu.edu.cn) (T. Suo).

activated equations. More recently, Somarathna et al. [13] considered a hyperelastic model with strain rate factor to predict the behaviour of polyurethane under varying strain rates and uniaxial tensile loading. Jahanmardi et al. [14] modified a hyper-viscoelastic damage evolution constitutive model with a dynamic increase factor for polyurethane materials. In general, the phenomenological constitutive models based on the hereditary integral approach [15] are very useful in describing the viscoelastic behaviour of polymers that change with deformation or time. Yang et al. [16] and Hoo Fatt et al. [17] proposed hyper-viscoelastic constitutive models, based on a hereditary integral law, to study the high strain rate response of rubber. However, the applicability of these models was limited due to the consideration of only one relaxation time or a constant memory function, which restricted their use to a narrow range of strain rates [18].

When an elastomer responds to high strain rates compared to low strain rates, the relaxation behaviour and experimental timescale of the deformation history are noticeably different. In low-strain rate experiments ( $<1\text{ s}^{-1}$ ), the experimental timescale is typically measured from 0.1 to 1000 s, but in high-strain rate experiments ( $>100\text{ s}^{-1}$ ), the timescale is typically measured from 1 to 1000  $\mu\text{s}$  [19]. A significant change in the relaxation modulus from rubbery behaviour to leathery or glassy behaviour was induced as the strain rate increased during the loading process [20]. Glass transition plays a critical role in determining the dynamic behaviour of polymers. Liu et al. [21,22] developed viscoelastic constitutive relationships using a dynamic hysteresis model and a spinodal model, to connect dynamic phase transitions to the thermomechanical processes. Physically based viscoelastic constitutive models developed by Amirkhizi et al. [23] and Clifton et al. [24] were introduced to capture the observed nonlinear mechanical response at high pressures and high strain rates. This method is more suitable for developing the viscoelastic constitutive models with a continuous distribution of effective relaxation times.

An alternative approach of interest is to extend the well-known rheological models to the large strain regime [25]. The generalised Maxwell viscoelastic model or the Weichert model is limited in the linear viscoelasticity regime, and relaxation effects are typically characterised by Prony-series representations, containing a large number of material parameters. An internal variable approach was proposed by Simo [26], Holzapfel [27] and Tayeb et al. [28] in which the evolution of the rate-dependent viscous stress is defined directly by a rate differential equation that reflects the relaxation process occurring in rheological theory. Haupt and Lion [29] applied the concept of continuous relaxation spectrum to finite linear viscoelasticity. Reese et al. [30] presented a model for finite deformation viscoelasticity that utilizes a nonlinear evolution law.

The determination of constitutive parameters for the relaxation modulus is required to accurately simulate the viscoelastic deformation of materials [31]. Experimental investigations are typically employed to determine the relaxation functions. Goh et al. [32] introduced a simple method for computing the strain and the time-dependent constants of a non-linear viscoelastic materials model with monotonic compression and stress relaxation tests. The common method for determining viscoelastic behaviour is the large-deformation step strain relaxation test [33], in which the stress decays over time with the applied step strain loading. However, this approach lacks sufficient accuracy in describing the relaxation process when the relaxation time is shorter than the ramp loading duration [34]. Owing to the limitation of the relaxation test, the relaxation constants for a higher strain rate loading cannot be determined using this method.

A novel experimentally-based method provided by Jia et al. [35] and Esposito [36] was applied to obtain a time-dependent relaxation modulus with dynamic mechanical analysis (DMA) and relaxation spectrum. DMA is generally more accurate for studying relaxation behaviour over a wide time or frequency range and obtaining an experimental-based relaxation function [37,38]. With the aid of time-temperature superposition principle (TTSP), the relaxation modulus

corresponding to a wide range of frequencies or timescales can be elucidated. The main advantage of this method is that the viscoelastic parameters can be directly identified from standard DMA tests of polymeric elastomers without extremely difficult optimization problems [28]. Viscoelastic parameters in a Prony series model are often determined using mathematical algorithms, such as the least-squares method [39] and the collocation method [40]. However, the accuracy of the collocation method depends on the careful selection of data points, which are divided into multiple time segments across the entire time domain. The least-squares method remains an ill-posed mathematical problem and cannot avoid negative parameter-fitting results.

This paper proposes a hyper-viscoelastic model to capture the nonlinear large deformation and rate-sensitivity of polymers. The hyper-viscoelastic model is achieved by incorporating the viscoelasticity at a finite strain and utilising internal state variables. The development of finite viscoelasticity is based on the concept of internal variables and the rate evolution equation. A linear rate evolution equation that governs the internal state of the material is used to modify the rate-dependent viscous response. The constitutive model combines a rate-independent nonlinear elastic function with a time-dependent linear relaxation function. A separable parameter-determination method was developed to provide experimentally based hyperelastic constitutive relations and linear viscoelastic properties to capture the rate-dependent behaviour. The viscoelastic parameters were determined using a continuous relaxation spectrum. Finally, the nominal stress-strain curves ( $0.001\text{--}5000\text{ s}^{-1}$ ) obtained from the experimental results were compared with results predicted by the constitutive models. This paper introduces a novel approach to characterise the rate-dependent properties of polyurethanes. Our work also offers an efficient method for experimentally determining viscoelastic parameters using a continuous spectrum.

## 2. Framework for the hyper-viscoelastic constitutive model

### 2.1. Basic theory

The generalised Maxwell or Weichert model, which is constructed using the parallel connection of a spring element and a series of Maxwell elements, is commonly employed to characterise the mechanical behaviour of viscoelastic materials [41]. The model is characterised by the elastic modulus  $E_\infty$ , and viscosity  $\eta_i$ , as depicted in Fig. 1(a). The applied stress  $\sigma$  is expressed as follows:

$$\sigma = E_\infty \epsilon + \sum_{i=1}^N q_i \quad (1)$$

where the total strain is denoted by  $\epsilon$ . The internal stresses induced by viscosity and the inelastic strains in the dashpot of the  $i$ -th Maxwell elements are denoted as  $q_i$  and  $\alpha_i$ , and their relationship is

$$q_i(t) = \eta_i \dot{\alpha}_i(t) = E_i(\epsilon - \alpha_i) \quad (2)$$

The evolution equations for the internal stresses  $q_i$  can be derived by differentiating with respect to time, as follows:

$$\dot{q}_i(t) + \frac{q_i}{\tau_i} = \frac{d}{dt}(E_i \epsilon) \quad (3)$$

where the relaxation times are denoted as  $\tau_i = \eta_i/E_i$ .

The response of total stress in Eq. (1) is split into the elastic and viscous parts, in which the elastic part is using the classical Hooke's law, while the viscous part can be written in an integral form as follows:

$$\sigma(t) = E_\infty \epsilon + \sum_{i=1}^N E_i \int_0^t \exp\left(\frac{t-s}{\tau_i}\right) \dot{\epsilon}(s) ds \quad (4)$$

Hence, the total stress in Eq. (4) can be derived as follows:

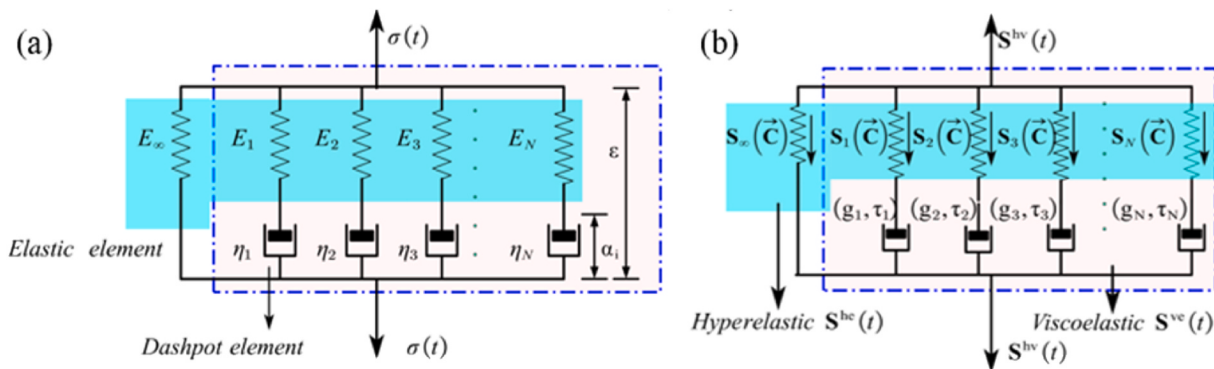


**Fig. 1.** Schematic of the hyper-viscoelastic model: generalised Maxwell model(a) and modified generalised Maxwell model (b).

$$\sigma(t) = E_0 \int_0^t g(t-s) \dot{\epsilon}(s) ds \quad (5)$$

where the instantaneous elastic modulus is denoted by  $E_0 = E_\infty + \sum_{i=1}^N E_i$ .

For such viscoelastic materials, the dimensionless function  $g(t)$ , which considers the time-dependent behaviour, is expressed by the Prony series as follows:

$$g(t) = g_\infty + \sum_{i=1}^N g_i \exp(-t/\tau_i) \quad (6)$$

where  $g_\infty$  is the dimensionless coefficient for the equilibrium response,  $g_i$  denotes the dimensionless coefficients for the viscous response, and  $\tau_i$  denotes the relaxation times.

The dimensionless function  $g(t)$  is formed by summing the decaying exponential functions of time, and these material parameters are grouped as a set  $[g_i, \tau_i]$ , called the discrete relaxation spectrum (DRS). As a requirement for Prony series convergence, each viscous coefficient  $g_i$  should be positive and less than 1, and these restrictions can be expressed as

$$g_\infty + \sum_{i=1}^N g_i = 1, g_\infty > 0, g_i \geq 0. \quad (7)$$

Furthermore,  $g(t)$  can be related to a fundamental material property with the continuous relaxation spectrum (CRS) [41,42] as the following equation:

$$\begin{aligned} g(t) &= g_\infty + \int_0^\infty \frac{\hat{H}(\tau)}{\tau} e^{-t/\tau} d\tau \\ &= g_\infty + \int_0^\infty \hat{H}(\tau) e^{-t/\tau} d \ln \tau. \end{aligned} \quad (8)$$

In the context of viscoelastic behaviour, the relaxation modulus function represents the time-dependent behaviour. The relaxation spectrum is characterized by a continuous logarithmic distribution of relaxation times, which is a fundamental aspect of the Prony series model in physics. Then, Eq. (8) is integrated to transform the time dimension of the relaxation spectrum into a logarithmic scale. To develop the Prony series models of Eq. (6) based on the established continuous relaxation spectrum  $\hat{H}(\tau)$ , we can approximate the form of the Prony series as

$$g(t) \cong g_\infty + \sum_{i=1}^N \hat{H}(\tau_i) \exp(-t/\tau_i) (\Delta \ln \tau_i) \quad (9)$$

where the relaxation times are selected to be equally spaced on a logarithmic timescale, denoted as

$$\tau_1 < \tau_2 < \dots < \tau_N \quad (10)$$

The distance between two adjacent points is represented by  $\Delta \ln \tau_i$ . Calculating the normalised relaxation modulus in Eqs. (5) and (9) involves utilising the intensities of the relaxation spectrum as follows:

$$g_i = \hat{H}(\tau) \cdot (\Delta \ln \tau_i) \quad (11)$$

## 2.2. Constitutive model

To generalise the above model to a large-strain case, we characterise the viscoelastic properties by super-positioning nonlinear spring and viscous dashpot elements, as Fig. 1(b). The rheological illustration is modified by replacing the elastic spring elements with hyperelastic spring elements to conduct a large-strain analysis. The extension to nonlinear elasticity is accomplished by formulating a strain energy function that represents the total elastic energy stored in materials to characterise the initial nonlinear response of the material at large strains. In the modified generalised Maxwell model, the viscoelastic behaviour can be expressed using the same set of viscoelastic parameters  $[g_i, \tau_i]$ .

Based on the parallel structure of the generalised Maxwell viscoelastic model, we obtain a decoupled stress response consisting of both equilibrium and nonequilibrium components. The rate-independent equilibrium response is modelled using a nonlinear spring that represents hyperelasticity. The rate-dependent viscoelastic responses are modelled using a series of modified Maxwell elements. The total stress includes a long-term or equilibrium stress and a series of nonequilibrium stresses. The parallel arrangement of long-term hyperelastic and rate-dependent viscoelastic components results in an additive combination for calculating the total hyper-viscoelastic stress as

$$\mathbf{S}^{hv}(\mathbf{C}, t) = \mathbf{S}_\infty^{he}(\mathbf{C}) + \sum_{i=1}^N \mathbf{S}_i^{ve}(\mathbf{C}, t) \quad (12)$$

where the superscripts  $\infty$ ,  $he$ ,  $ve$ , and  $hv$  denote the long-term, hyperelasticity, viscoelasticity, and hyper-viscoelasticity, respectively.

The hyper-viscoelastic model presented in this paper is within the framework of rational thermodynamics and the internal state variable approach. With reference to the traditional continuum analysis, a mechanical framework for finite deformation under isothermal conditions is outlined. A macroscopic motion between the reference configuration and the deformed configuration is denoted as  $\Phi$ . The deformation gradient and the Jacobian of the deformation gradient tensor are denoted as

$$F = dx/dX, J = \det[F]. \quad (13)$$

The deviatoric part of the deformation gradient tensor is represented by  $\bar{\mathbf{F}} = J^{-1/3} \mathbf{F}$ . For nearly incompressible isotropic nonlinear viscoelastic solids,  $J = 1$ . The right Cauchy–Green tensors together with their principal invariants are expressed as:

$$\bar{\mathbf{C}} = \bar{\mathbf{F}}^T \bar{\mathbf{F}} = J^{-2/3} \mathbf{C} \quad (14)$$

$$\bar{I}_1 = \text{tr}(\bar{\mathbf{C}}), \bar{I}_2 = \frac{1}{2} - [\text{tr}(\bar{\mathbf{C}})^2 - \text{tr}(\bar{\mathbf{C}}^2)], \bar{I}_3 = \det(\bar{\mathbf{C}}) = 1 \quad (15)$$

The instantaneous elastic stress tensor is denoted as:

$$\mathbf{S}_0(\mathbf{C}) = 2 \frac{\partial W^0(\mathbf{C})}{\partial \mathbf{C}}. \quad (16)$$

The elastic energy stored in a material under finite deformation is defined by the initial instantaneous strain energy function:

$$W^0(\mathbf{C}) = U(J) + \bar{W}^0(\mathbf{C}) \quad (17)$$

where  $U(J)$  and  $\bar{W}^0(\bar{\mathbf{C}})$  are the volumetric and deviatoric components of the total strain energy function, respectively.

In Eqs. (16) and (17), the instantaneous stress tensor is expressed as

$$\mathbf{S}_0(\mathbf{C}) = 2 \frac{\partial W^0(\mathbf{C})}{\partial \mathbf{C}} = 2 \frac{\partial U}{\partial J} \frac{\partial J}{\partial \mathbf{C}} + 2 \frac{\partial \bar{W}^0(\mathbf{C})}{\partial \mathbf{C}} : \frac{\partial \bar{\mathbf{C}}}{\partial \mathbf{C}} \quad (18)$$

and the applications of the chain rule yield the following relationships:

$$\begin{aligned} \partial J / \partial \mathbf{C} &= \frac{1}{2} J \mathbf{C}^{-1} \\ \partial \bar{\mathbf{C}} / \partial \mathbf{C} &= J^{-2/3} \left[ \mathbf{I} - \frac{1}{3} \mathbf{C} \otimes \mathbf{C}^{-1} \right] \end{aligned} \quad (19)$$

With assuming a purely elastic response in the bulk, the instantaneous stress tensor can be split into the pressure and deviator terms and expressed as follows:

$$\mathbf{S}_0(\mathbf{C}) = J p \mathbf{C}^{-1} + \text{dev} \mathbf{S}_0(\mathbf{C}) \quad (20)$$

where  $\text{dev}(\bullet) = (\bullet) - 1/3[\mathbf{I} : (\bullet)]\mathbf{I}$  denotes the deviator operator in the current configuration. Hence, the deviator term of the instantaneous stress tensor is expressed as follows:

$$\mathbf{S}_0^d(\mathbf{C}) = \text{dev} \mathbf{S}_0(\mathbf{C}) = J^{-2/3} \left[ \frac{\partial \bar{W}^0(\mathbf{C})}{\partial \mathbf{C}} - \frac{1}{3} \left( \mathbf{C} : \frac{\partial \bar{W}^0(\mathbf{C})}{\partial \mathbf{C}} \right) \mathbf{C}^{-1} \right] \quad (21)$$

here, the deviator term of Eq. (21) is split into an equilibrium elastic response with the dimensionless coefficient  $g_\infty$  and a series of non-equilibrium viscous responses with dimensionless coefficients  $g_i$  [25, 27, 28]. The equilibrium elastic response is expressed as

$$\mathbf{S}_{\infty}^{he}(\mathbf{C}) = g_\infty \mathbf{S}_0^d. \quad (22)$$

An extension of the internal variables derived from the rate evolution function is employed to establish a rate-dependent viscous response. To incorporate the relaxation of stress in response to a sudden change in strain, we consider the viscous behaviour of stress in the dashpot element of each Maxwell branch as an internal variable,  $\mathbf{Q}_i$ . The mechanical relationship of the Maxwell element is generalised to a finite deformation regime, resulting in a newly developed rate equation. This equation that governs the evolution of the internal variables is

$$\frac{\partial \mathbf{Q}_i}{\partial t} + \frac{1}{\tau_i} \mathbf{Q}_i = \frac{g_i}{\tau_i} \mathbf{S}_0^d(\mathbf{C}) \quad (23)$$

By introducing a factor  $\exp(t/\tau_i)$  on both sides of Eq. (23), the evolution equation for the internal variable  $\mathbf{Q}_i(t)$  can be integrated. The result yields a closed-form convolution solution as expressed:

$$\mathbf{Q}_i(t) = g_i \int_{-\infty}^t \exp\left[\frac{(t-s)}{\tau_i}\right] \frac{d}{ds} [\mathbf{S}_0^d(\mathbf{C}, s)] ds \quad (24)$$

Coleman et al. [43] have discussed the Calusius-Duhem inequality in the thermodynamics constitutive model. The free energy function and stress of materials should be satisfied for thermodynamic consistency as follows:

$$-W^0(\mathbf{C}, \mathbf{Q}) + \frac{1}{2} \mathbf{S} : \dot{\mathbf{C}} \geq 0, \quad (25)$$

where  $W^0$  is the free energy equation with all of internal variables. The inequality formulation in Eq. (25) leads to the expression of intrinsic dissipation as follows:

$$\frac{\partial W^0(\mathbf{C}, \mathbf{Q})}{\partial \mathbf{Q}} : \dot{\mathbf{Q}} \geq 0 \quad (26)$$

The constitutive model of stress can be achieved by the former equation,

$$\mathbf{S} = \frac{1}{2} \frac{\partial W^0(\mathbf{C}, \mathbf{Q})}{\partial \mathbf{C}}. \quad (27)$$

Hence, the total stress tensor in the form of the second Piola-Kirchhoff stress tensor, is expressed as follows:

$$\mathbf{S}^{hv}(t) = J p \mathbf{C}^{-1} + g_\infty \mathbf{S}_0^d + \sum_{i=1}^N \mathbf{Q}_i(t). \quad (28)$$

Consequently, the visco-hyperelastic constitutive description is presented as:

$$\mathbf{S}^{hv}(t) = J p \mathbf{C}^{-1} + g_\infty \mathbf{S}_0^d(t) + \sum_{i=1}^N g_i \int_{-\infty}^t \exp[(t-s)/\tau_i] \frac{d}{ds} [\mathbf{S}_0^d(s)] ds. \quad (29)$$

Therefore, the overall stress experienced by a hyper-viscoelastic solid elastomer can be composed of a rate-independent hyperelastic component and a rate-dependent viscoelastic component in a discrete stress-strain relationship.

### 2.3. Time integration method

In addition, the subsequent procedure presents a recursive method for the time integration and updating of the internal variables in Eq. (24). In previous studies, a direct time-step increment approach was used to approximate the convolution integral for stress determination [44, 45].

The following section outlines the numerical approach used to compute the convolution integrals associated with the time-dependent viscoelastic response. The fundamental concept is to convert the convolution representation into a sequence of recursively updated equations incorporating Eq. (29). Consider a partition of a time interval of interest, denoted by  $[0, T]$ , and a subinterval, denoted by  $[t_n, t_{n+1}]$ , where represents the time increment between the previous step time and the current step time  $t_{n+1}$ . This interval is subdivided into  $n$  increments as follows:

$$[0, T] = \bigcup_n [t_n, t_{n+1}], t_{n+1} = t_n + \Delta t. \quad (30)$$

The evolution equation for internal variables  $\mathbf{Q}_i(t)$  in Eq. (24) can be divided into two parts, as follows:

$$\begin{aligned} \mathbf{Q}_i(t_{n+1}) &= \int_0^{t_n} \exp[-(t_n-s)/\tau_i] \frac{d}{ds} (\mathbf{S}_0^d(s)) ds + \int_{t_n}^{t_{n+1}} \exp[-(t_{n+1}-s)/\tau_i] \frac{d}{ds} (\mathbf{S}_0^d(s)) ds. \end{aligned} \quad (31)$$

The exponential function is assumed to satisfy the following standard property:

$$\exp[(t_n + \Delta t)/\tau_i] = \exp(\Delta t/\tau_i) \exp(t_n/\tau_i). \quad (32)$$

The approximation of diffraction of deviatoric instantaneous stress [32] is

$$\frac{d}{ds} (\mathbf{S}_0^d(s)) = \lim_{\Delta s \rightarrow 0} \frac{\mathbf{S}_0^d(s) - \mathbf{S}_0^d(t_n)}{\Delta s} = \lim_{\Delta t \rightarrow 0} \frac{\mathbf{S}_0^d(t_{n+1}) - \mathbf{S}_0^d(t_n)}{\Delta t}. \quad (33)$$

Considering that all quantities are known at time  $t_n$ , and all strain quantities are known at time  $t_{n+1}$ , a recursive incremental formula for the internal state value can be deduced:

$$\begin{cases} \mathbf{Q}_i(t_{n+1}) = \alpha_i \mathbf{Q}_i(t_n) + \beta_i [\mathbf{S}_0^d(t_{n+1}) - \mathbf{S}_0^d(t_n)] \\ \alpha_i = \exp(-\Delta t/\tau_i) \\ \beta_i = g_i \frac{1 - \exp(-\Delta t_n/\tau_i)}{\Delta t_n/\tau_i} \end{cases} \quad (34)$$

Here, we present the final formulation of the model by extending the well-known linear rheological models to the large strain regime with a representation of the relaxation spectrum. As shown in Fig. 2, this paper introduces a constitutive model that presents a comprehensive theoretical framework diagram that encompasses the three main features of mechanical deformation observed in polyurethane elastomers. These aspects are (1) the exhibition of nonlinear hyperelastic behaviour at large strains, as described by an energy density function; (2) the dependence on strain rate, which is governed by a rate evolution function; (3) the time-dependent relaxation behaviour, which is characterised by a relaxation spectrum. A recursive update procedure is developed to calculate the total hyper-viscoelastic response. By understanding and modelling these responses, researchers can gain valuable insights into the properties and viscoelastic behaviours of polymer elastomers, which can then be utilised to optimise their performance in various applications.

### 3. Model identification

This section describes a systematic procedure for identifying the material parameters of the proposed hyper-viscoelastic model. A comprehensive characterisation of polymeric materials often requires multiple parameters to be considered owing to their hyper-viscoelastic behaviour. These parameters are typically determined by applying an evolutionary strategy that enables the separation of long-term and stress-relaxation behaviours. The detailed identification of the

hyperelastic strain energy-density function is based on the long-term hyperelastic response. The identification of the viscoelastic relaxation function is based on the conversion of the continuous spectrum.

#### 3.1. Compression behaviour with homogeneous uniaxial deformations

Consider a viscoelastic body undergoing a simple uniaxial homogeneous deformation referred to in the reference and deformed configurations. The deviatoric part of the instantaneous stored elastic energy density in Eq. (17) is expressed as the Mooney–Rivlin function based on only three parameters [46]:

$$\bar{W}^0(\mathbf{C}) = A_{10}(\bar{I}_1 - 3) + A_{01}(\bar{I}_2 - 3) + A_{11}(\bar{I}_1 - 3)(\bar{I}_2 - 3). \quad (35)$$

For a uniaxial experiment, the ratio of the initial length to the real-time length is denoted as  $\lambda$  and is determined by the uniaxial compression strain:  $\lambda = 1 - \epsilon_{11}$ . The stretch ratios are  $\lambda_1 = \lambda, \lambda_2 = \lambda_3 = \sqrt{\lambda}$ . The deformation gradient tensor and corresponding strain tensor for incompressible materials are expressed by the stretch ratios as follows:

$$\mathbf{F} = \text{diag}(\lambda, \lambda^{-1/2}, \lambda^{-1/2}), \mathbf{C} = \text{diag}(\lambda^2, \lambda^{-1}, \lambda^{-1}). \quad (36)$$

The second Piola–Kirchhoff stress tensor in Eq. (19) is simplified as the first Piola–Kirchhoff stress tensor with the following relationship:  $\mathbf{II}(t) = \mathbf{FS}(t)$ . The first Piola–Kirchhoff stress tensor is the ratio of the measured force to the reference area and the principal stretch. In uniaxial deformation, the first Piola–Kirchhoff stress is represented by the nominal stress, which is calculated by dividing the actual force by the initial area.

From Eq. (35), the nominal stress with hydrostatic pressure term is expressed as

$$\Pi^0(t) = -p_0 \mathbf{F}^{-T} + \frac{\partial \bar{W}^0}{\partial \mathbf{F}} \quad (37)$$

Introducing the principal stretch ratios, the formulation above leads to

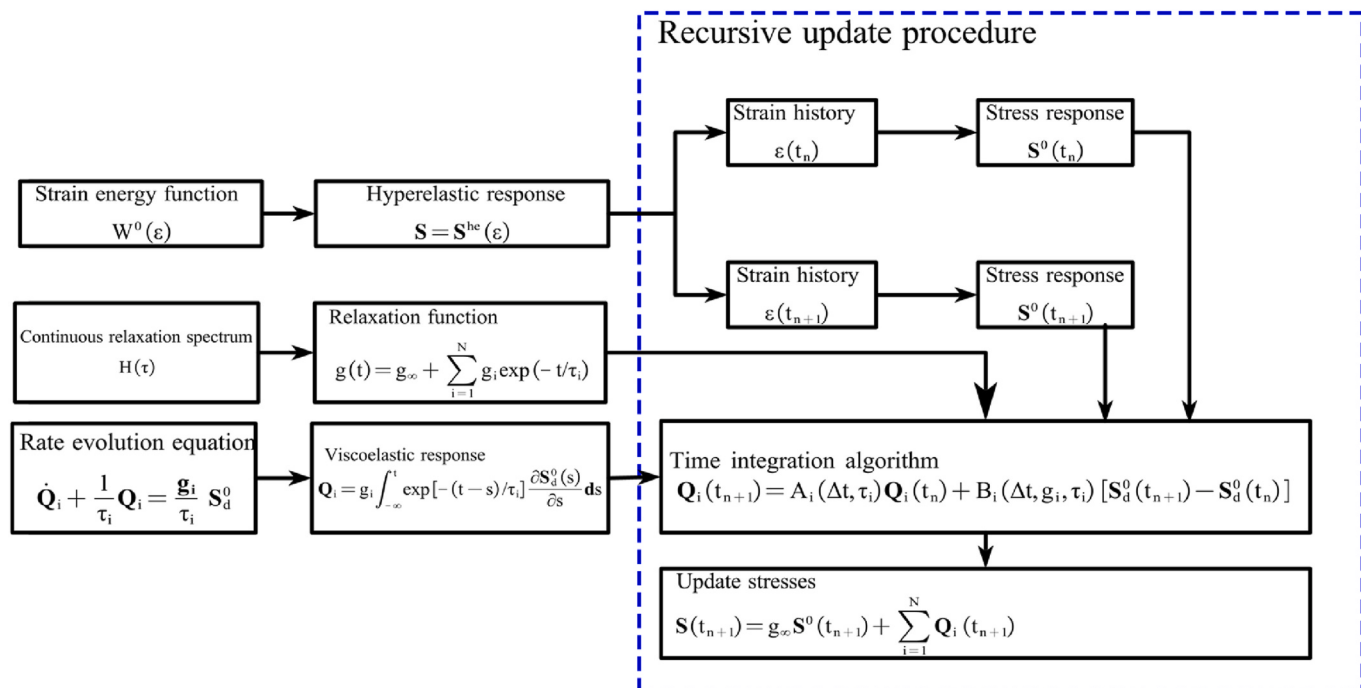


Fig. 2. Theoretical framework.

$$\begin{cases} \boldsymbol{\Pi}_{11}^0(t) = -\frac{p_0}{\lambda_1} + \frac{\partial \bar{W}}{\partial \lambda_1} \\ \boldsymbol{\Pi}_{22}^0(t) = -\frac{p_0}{\lambda_2} + \frac{\partial \bar{W}}{\partial \lambda_2} \\ \boldsymbol{\Pi}_{33}^0(t) = -\frac{p_0}{\lambda_3} + \frac{\partial \bar{W}}{\partial \lambda_3} \end{cases} \quad (38)$$

Because of the incompressible assumption, the partial derivatives of  $\bar{W}$  with respect to  $\lambda_m$  ( $m = 1, 2$  and  $3$ ) can be written as follows:

$$\frac{\partial \bar{W}}{\partial \lambda_m} = \frac{\partial \bar{W}}{\partial \bar{I}_1} \frac{\bar{I}_1}{\partial \lambda_m} + \frac{\partial \bar{W}}{\partial \bar{I}_2} \frac{\bar{I}_2}{\partial \lambda_m} \quad (39)$$

The boundary conditions for the uniaxial compression [44] are as follows:

$$\boldsymbol{\Pi}_{22}^0(t) = \boldsymbol{\Pi}_{33}^0(t) = 0. \quad (40)$$

Substituting the boundary conditions into Eq. (38) to reduce the pressure term, the instantaneous stress with the three parameters from the strain-energy function in Eq. (35) is expressed as follows:

$$\boldsymbol{\Pi}_{11}^0(\lambda) = 2(\lambda - \lambda^{-2}) [\Lambda_{10}\lambda + \Lambda_{01} + \Lambda_{11}(\lambda^2 + 2\lambda^{-1} - 3) + \Lambda_{11}\lambda(\lambda^{-2} + 2\lambda^{-1} - 3)] \quad (41)$$

The total stress with all internal variables is expressed as:

$$\boldsymbol{\Pi}_{11}(t) = g_\infty \boldsymbol{\Pi}_{11}^0 + \sum_{i=1}^N g_i \int_0^t \exp[-(t-s)/\tau_i] \frac{d}{ds} (\boldsymbol{\Pi}_{11}^0(s)) ds \quad (42)$$

By consideration of the recursive incremental formula presented in Eq. (34), the rate-dependent deformation response with internal variables for uniaxial loading is expressed as follows:

$$\begin{cases} \boldsymbol{\Pi}_{11}(t_{n+1}) = \alpha_i \boldsymbol{\Pi}_i(t_n) + \beta_i [\boldsymbol{\Pi}_{11}^0(t_{n+1}) - \boldsymbol{\Pi}_{11}^0(t_n)], \\ \alpha_i = \exp(-\Delta t/\tau_i), \\ \beta_i = g_i \frac{1 - \exp(-\Delta t_n/\tau_i)}{\Delta t_n/\tau_i}. \end{cases} \quad (43)$$

Under the conditions of very slow deformation rates, the equilibrium response can be deduced. Quasi-static uniaxial tests conducted at strain rates below  $10^{-2} \text{ s}^{-1}$  is assumed that the material response is essentially rate-independent [46]. Under this condition, time approaches infinity and the long-term response can be described as:

$$\boldsymbol{\Pi}_{11}^\infty(\lambda) = g_\infty \boldsymbol{\Pi}_{11}^0 = 2(\lambda - \lambda^{-2}) [\bar{\Lambda}_{01} + \bar{\Lambda}_{10}\lambda + \bar{\Lambda}_{11}((\lambda^2 + 2\lambda^{-1} - 3) + \lambda(\lambda^{-2} + 2\lambda^{-1} - 3))] \quad (44)$$

where the parameters in long-term response, denoted as  $\bar{\Lambda}_{10}$ ,  $\bar{\Lambda}_{01}$ ,  $\bar{\Lambda}_{11}$ , are defined as

$$\begin{cases} \bar{\Lambda}_{10} = g_\infty \Lambda_{10}, \\ \bar{\Lambda}_{01} = g_\infty \Lambda_{01}, \\ \bar{\Lambda}_{11} = g_\infty \Lambda_{11}. \end{cases} \quad (45)$$

A combination of all rate-dependent stresses (Eq. (43)) and rate-independent stress (Eq. (44)) is deduced from the recursive update procedure. Consequently, a total stress result is expressed as:

$$\boldsymbol{\Pi}_{11}(t_{n+1}) = g_\infty \boldsymbol{\Pi}_{11}^0(t_{n+1}) + \sum_{i=1}^N \boldsymbol{\Pi}_i(t_{n+1}) \quad (46)$$

### 3.2. Viscoelastic behaviour

#### 3.2.1. Characterization using dynamic mechanical analysis

Viscoelastic phenomena can be described by three basic viscoelastic material functions, including: relaxation modulus, creep compliance, as well as complex modulus [40]. The viscoelastic complex modulus  $E^*$ ,

and the loss angle,  $\tan \delta$ , are characterized using dynamic mechanical analysis. In dynamic mechanical analysis, the stretch history with imposed dynamic deformation with the stress response at the loading frequency is defined by the following expression:

$$\lambda(t) = 1 + a_o \sin \omega t \quad (47)$$

$$\sigma(\omega) = a_o E^*(\omega) \quad (48)$$

where  $\omega$  is the loading frequency and  $a_o$  is a small amplitude of deformation. The complex modulus  $E^*$  can be determined by measuring the deformation amplitude and phase-lag  $\delta$  between the stress and strain sine waves. Furthermore, the storage modulus  $E'$  and loss modulus  $E''$  components decomposed by the complex modulus  $E^*$  are expressed as follows:

$$\begin{cases} E'(\omega) = |E^*(\omega)| \cos \delta, \\ E''(\omega) = |E^*(\omega)| \sin \delta, \\ \tan \delta = E''(\omega)/E'(\omega). \end{cases} \quad (49)$$

The storage and loss moduli represent the dynamic stiffness and the ability to dissipate mechanical energy, respectively. The loss factor, which is defined as the ratio of the loss modulus to the storage modulus, quantifies the proportion of mechanical energy that is dissipated and stored during each loading cycle.

#### 3.2.2. Mathematical model of master curve

A master curve can be built by applying the time-temperature superposition principle [37, 41, 47, 48]. Application of the TTSP allows further extension of the measurement range, which is a powerful tool to strongly extend the viscoelastic behaviour over a wide range of frequencies, from relatively low-frequency response to high-frequency response. With the aid of TTSP, the frequency-dependent representation can be effectively achieved in a standardized master curve within the field of polymer physics.

In this paper, the continuous time-dependent sigmoidal function [49, 50] has been successful in characterising the viscoelastic behaviour of polymers and is employed to construct the master curve  $E'(\omega)$ . The expression of storage modulus with sigmoidal function is present as follows:

$$\lg E'(\omega) = \delta_s + \frac{\alpha_s}{1 + \exp(\beta_s + \gamma_s \lg \omega)} \quad (50)$$

where  $\delta_s$  is the logarithm of the storage modulus in a rubbery state,  $\alpha_s$ ,  $\beta_s$  and  $\gamma_s$  are shape coefficients.

#### 3.2.3. Continuous relaxation spectrum

The relaxation moduli in the time or frequency domains within a mathematical model are closely interrelated through the corresponding relaxation spectrum [51]. A continuous spectrum, which refers to the distribution of relaxation time, is a fundamental characteristic of a viscoelastic material [41, 52]. The continuous spectrum approach [53] is a practical method for directly deriving the relaxation functions of elastomers from frequency-domain master curves. This method employed the aforementioned approach to acquire a continuous relaxation spectrum by utilising the frequency-domain master curves, which could be obtained through experimental frequency sweep tests with DMA. Based on the analysis, the function or distributions of relaxation time, as the fundamental characteristics of the viscoelastic material, can be converted from the frequency domain with the continuous spectrum.

Tschoegl [42] obtained the following form of viscoelastic materials from the storage modulus function. The continuous relaxation spectrum defined in the frequency domain, is determined by the Fuoss–Kirkwood relation [52], as follows:

$$\begin{cases} H(\tau) = \pm \left( \frac{2}{\pi} \right) \text{Im}E'(\omega) \\ \omega = \tau^{-1} \exp\left(\pm \frac{j}{2}\right) \end{cases} \quad (51)$$

With this Fuoss–Kirkwood relation, the continuous spectrum  $H(\tau)$  is derived directly from the fitted sigmoid function of the master curve  $E'(\omega)$  using the inverse integral transform method [49]. And a more comprehensive relaxation spectrum corresponding to the sigmoid function is expressed as follows:

$$\begin{cases} H(\tau) = -\frac{2}{\pi} \exp(X(\tau)) \sin(Y(\tau)) \\ X(\tau) = k_1 + \frac{k_2 \left[ e^{-(k_3 - k_4 \ln \tau)} + \cos\left(\frac{\pi}{2}k_4\right) \right]}{e^{-(k_3 - k_4 \ln \tau)} + e^{(k_3 - k_4 \ln \tau)} + 2 \cos\left(\frac{\pi}{2}k_4\right)} \\ Y(\tau) = \frac{k_2 \sin\left(\frac{\pi}{2}k_4\right)}{e^{-(k_3 - k_4 \ln \tau)} + e^{(k_3 - k_4 \ln \tau)} + 2 \cos\left(\frac{\pi}{2}k_4\right)} \end{cases} \quad (52)$$

where  $X(\tau)$  and  $Y(\tau)$  are the real part and imaginary part of a complex quantity. The parameters of the sigmoid function in Eq. (50) are subsequently returned to determine the parameters of the natural logarithm, as indicated:

$$\begin{cases} k_1 = \delta_s \ln 10, \\ k_2 = \alpha_s \ln 10, \\ k_3 = \beta_s, \\ k_4 = \gamma_s / \ln 10. \end{cases} \quad (53)$$

Therefore, with Eqs. (52) and (53), the continuous form of the relaxation spectrum can be derived from a set of parameters, which is obtained through the experimental data of dynamic modulus testing.

Furthermore, the continuous relaxation spectrum is the basic representation of the viscoelastic behaviour of polymer materials and the bridge between time-domain and frequency-domain viscoelastic behaviour. The identification and utilisation of continuous spectra derived from experimental data in the development of constitutive models are vital because they represent the fundamental nature of the relaxation phenomenon in various loading conditions. In addition, two main assumptions should be employed to predict viscoelastic response at large strains: (1) the viscous stress follows the linear differential equations, as described in Eq. s (3) and (23); (2) the linear viscoelastic

relationship remains valid for both the small-strain and large-strain scenarios.

#### 4. Experiments

##### 4.1. Materials

Polyurethane elastomer specimens tested in this research were prepared by the Tiemao Glass Co., Ltd. The polyurethane elastomer was used as the interlayer material of the laminated glass. Polyurethane samples were based on methylene diphenyl diisocyanate, polyether polyol, and small molecule chain extender, with pouring and high-temperature curing process. Complete transparent polyurethane materials with the hardness of Shore A60, were prepared as compression moulded sheets.

##### 4.2. Compression tests

The schematic presentation of the experimental procedure is shown in Fig. 3. Compression tests are carried out on two different types of testing machines to cover a broad range of loading speeds: (1) a micro universal testing machine for low strain rate tests and (2) a modified split Hopkinson pressure bar system (SHPB) for high strain rate tests. Uniaxial compression tests were conducted over a wide range of strain rates using cylindrical rod specimens.

Related literature [54,55] indicates that polymer samples should have aspect ratios between 0.25 and 0.5 to effectively reduce wave attenuation and control frictional effects. Hence, the dimension of the rod samples used in the compression test is designed with a diameter of 6 mm and a thickness of 3 mm, as shown in Fig. 4(a). The samples were obtained from a transparent polyurethane sheet with a thickness of 3 mm using a steel-cutting machine.

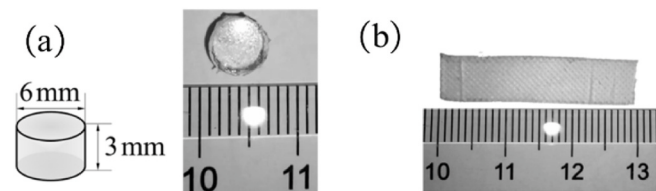


**Fig. 4.** Rod sample for the compressive test (a) and sheet sample for the DMA test(b).

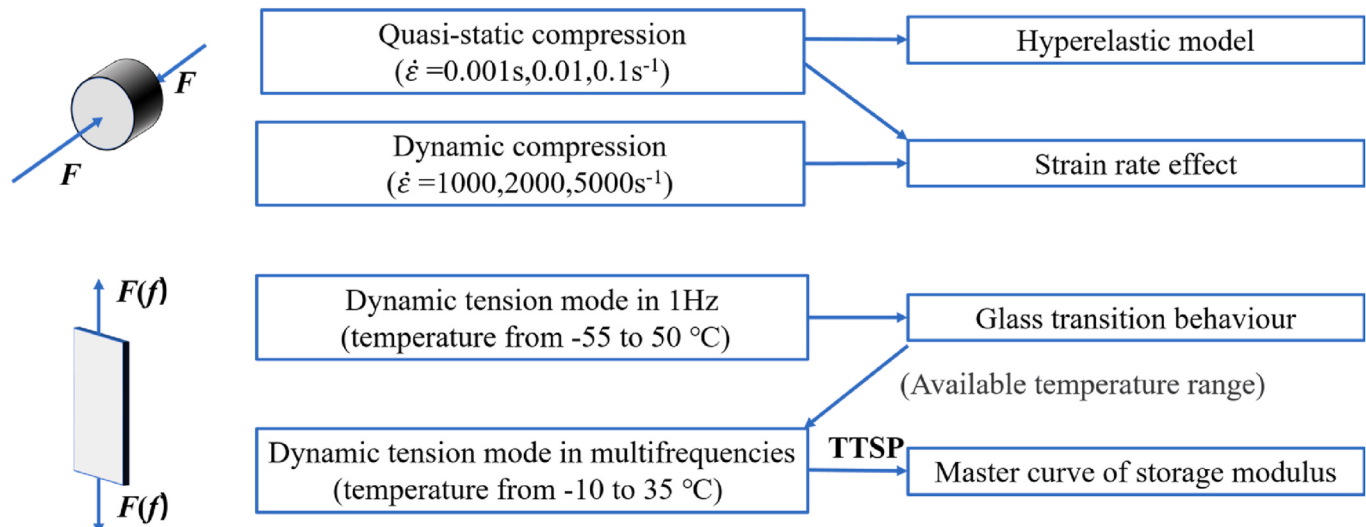


**Fig. 3.** Schematic of experimental procedure.

#### 4.2.1. Quasi-static compression tests

A micro universal testing machine (Instron 5848) was employed to conduct tests on the uniaxial compressive mechanical properties of polyurethane. The force applied during the testing procedure varied from 0.2 to 2000 N. The experimental investigation involved conducting tests at nominal strain rates of 0.001, 0.01, and 0.1 s<sup>-1</sup> while ensuring that the maximum achievable strain was set at 60%. A Vaseline lubricant was used between the specimen and compression plates to mitigate the effects of friction.

#### 4.2.2. High strain rate compression tests

This study used the SHPB system to investigate the compressive stress-strain behaviour of elastomers under high strain rates. The SHPB system is a well-established apparatus commonly used for high-strain rate testing. However, the direct application of this technique to the testing of polymeric materials has serious limitations [56,57]. Polyurethane material tends to exhibit low modulus at room temperature and a much lower wave impedance than metallic materials. The low impedance of polymers often results in a weak transmitted signal when a traditional metal transmitted bar is used, which poses a significant challenge in detecting the signal necessary to obtain stress-strain curves. Various methods to enhance the amplification are available, including opting for a strain gauge with a higher gain factor and utilising bars with a lower impedance, such as aluminium alloy, nylon or polymethyl methacrylate (PMMA) bars [58,59].

A configuration of the SHPB system is shown in Fig. 5. This system employed aluminium alloy pressure incident and transmission bars in order to reduce impedance mismatch. Axial strain gages mounted on the surfaces of the incident and transmission bars provided time-resolved measurements of the elastic strain pulses in the bars. The strain gauges were positioned at the midpoint of the incident bar and at a distance of 0.3 m from the interface between the transmission bar and the specimen. The original strain gages equipped on the incident and transmitted bars had a sensitivity factor of 1.92. In this study, the weakly transmitted signal was measured using a semiconductor strain gauge with a sensitivity factor of 110. The semiconductor strain gauge was placed on the transmitted bar to amplify the transmitted signal. The incident and reflected wave signals are shown in Fig. 6(a). As shown in Fig. 6(b), the transmission signal was significantly amplified by using high-sensitivity strain gauges.

During the SHPB test, the specimen was placed between two aluminium incident and transmitted bars. After undergoing multiple wave oscillations, the internal stress field of the specimen eventually reached equilibrium. The stress-strain relationship in the specimen was determined by analysing the strain history recordings of the bars. A detailed data analysis method was presented in the studies of Miao et al. [60]. Based on the elastic wave theory of one-dimensional wave propagation, the nominal strain rate and the axial strain of the sample were calculated as follows:

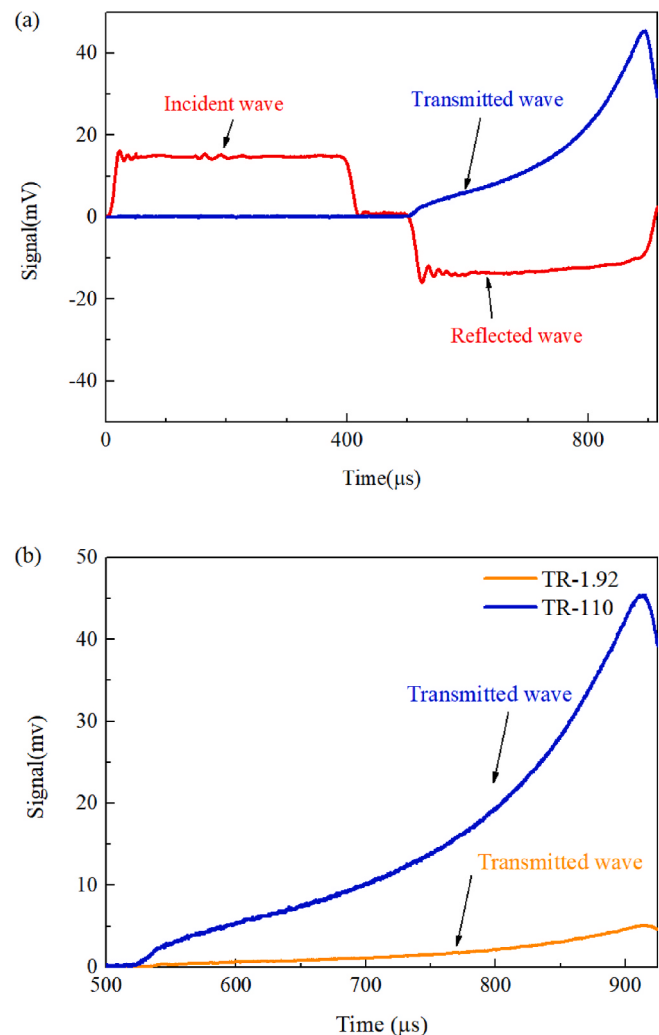


**Fig. 6.** Signals obtained from the SHPB: signals from the incident bar and transmitted bar (a) and signals of the transmitted bar captured using two different strain gauges(b).

$$\dot{\varepsilon}_N(t) = -\frac{2C_0}{l_0}\varepsilon_I(t) \quad (54)$$

$$\varepsilon_N(t) = \frac{2C_0}{l_0} \int_0^t \varepsilon_I(\tau) d\tau \quad (55)$$

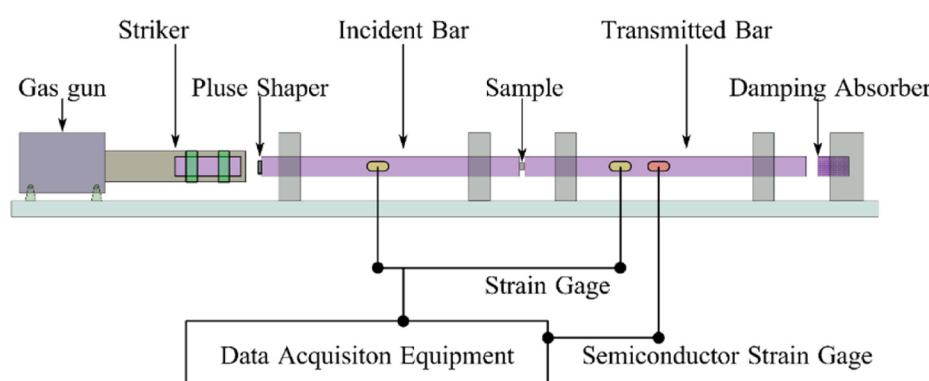


**Fig. 5.** Diagram of the split Hopkinson pressure bar (SHPB) device.

where  $C_0$  is the elastic wave velocity of the bar material,  $\varepsilon_i$  and  $\varepsilon_T$  are the strain signals of in the incident and transmitted wave pulses, and  $l_0$  is the initial length of samples. The nominal stress, also known as the engineering stress, can be determined using a constant initial area  $A_s$  of the specimen and the transmission strain signal  $\varepsilon_T(t)$  as follows:

$$\sigma_N = \frac{E_b A_b}{A_s} \varepsilon_T(t) \quad (56)$$

where the  $E_b$  and  $A_b$  are the elastic modulus and cross-sectional area of the transmission bar. The SHPB experiments were conducted with a strain rate range of  $1000\text{--}5000\text{ s}^{-1}$  and at a room temperature of  $20^\circ\text{C}$ .

#### 4.3. Tests on dynamic mechanical analysis

Dynamic mechanical experiments were conducted to investigate the viscoelastic behaviour of polyurethane elastomers over a wide range of frequencies and temperatures. The DMA tests were conducted using a dynamic mechanical analyser (Mettler Toledo 861e). Rectangular samples of thin film were normally tested in uniaxial tensile mode [8,61]. Specimens of rectangular geometry shown in Fig. 4(b) were machined with a total length of 30 mm, a width of 7 mm, and a thickness of 0.76 mm. For the tensile tests with this equipment, the applied force on the sample had a sensitivity factor of 1 mN. The gauge length was measured between the clamps, and the deformation amplitude was quantified using an LVDT displacement sensor. A gauge length of 19.5 mm was measured between clamps for mounting the samples.

As shown in Fig. 3, two types of dynamic mechanical tests were conducted to investigate the viscoelastic behaviour: (1) a temperature sweep test was conducted at a constant frequency of 1 Hz to examine the glass transition behaviour with temperature, and available temperature ranges for time-temperature superposition principle; (2) an isothermal multi-frequency test was conducted to examine the viscoelastic properties.

The temperature sweep test was conducted at a constant frequency of 1 Hz. The resulting behaviour of the material was documented. The temperature underwent a sweeping change, ranging from  $-55$  to  $50^\circ\text{C}$ , with a heating rate of  $3^\circ\text{C}$  per minute. A sinusoidal force was applied, resulting in a sinusoidal response of the sample in terms of strain. The displacement amplitude was set to  $5\text{ }\mu\text{m}$  to generate a strain amplitude of 0.25%. This amplitude was selected to ensure that the specimen remained in a linear viscoelastic state.

Isothermal multi-frequency sweep tests were conducted in the step-temperature mode. The temperature range for the experiments ranged from  $-10$  to  $35^\circ\text{C}$  (the region included the transition from glassy to rubbery state), with a temperature increment of  $5^\circ\text{C}$  for each test step. For each temperature increment, the temperature was maintained for a minimum of 10 min to ensure isothermal equilibrium. The oscillation frequencies of the nine points were logarithmically distributed with equal spacings between 1 and 100 Hz ( $f = 1, 1.778, 3.162, 5.623, 10, 17.28, 31.62, 56.23$ , and  $100\text{ Hz}$ ). The amplitude of the sinusoidal oscillation was consistent with that of the previous test. The storage modulus was recorded as a function of the frequency at each temperature increment.

## 5. Results and discussion

### 5.1. Results of compression tests

Here, a series of uniaxial compressive experiments were conducted across a wide range of strain rates to investigate the rate dependence of the polyurethane elastomer. A comprehensive characterisation of the stress-strain curves obtained from these compression experiments were presented in Figs. 7 and 8. With the increasing strain rate, the materials subjected to different strain-rate loading have shown the nonlinear elasticity at large deformations and the strain rate effect. Specifically,

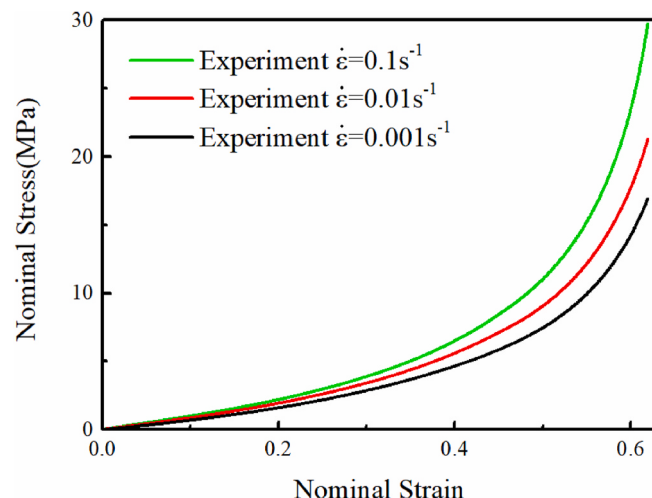


Fig. 7. Experimental results of the compressive tests under quasi-static conditions.

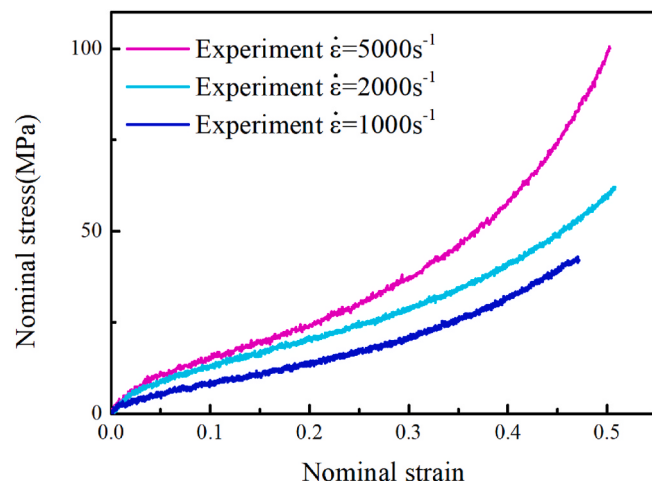


Fig. 8. Experimental results of the SHPB with a strain rate range of  $1000\text{--}5000\text{ s}^{-1}$ .

the stress on these materials increases significantly as the strain rate increases.

Generally, the rate-dependent behaviour of materials can be described by the dynamic increase factor (DIF) and Cowper-Symonds equation [13]. As shown in Fig. 9, DIF was obtained from the nominal stress at nominal strain 0.3 of various stress-strain curves, with the curve under strain rate  $0.001\text{ s}^{-1}$  as reference. The Cowper-Symonds equation is expressed as follows:

$$DIF = 1 + \left( \frac{\dot{\varepsilon}}{D} \right)^{\frac{1}{q}} \quad (57)$$

where  $D$  and  $q$  in Eq. (57) were then obtained as 342.7 and 3.104, respectively. As indicated in Fig. 9, DIFs are close to 1 for the strain rate range:  $0.0001\text{ s}^{-1}\text{--}0.1\text{ s}^{-1}$ . Therefore, the material can be considered as rate-independent at low strain rates.

### 5.2. Determination of parameters for hyperelastic behaviour

The long-term response in the hyper-viscoelastic model is the rate-independent response of materials at the equilibrium state. As stated in Section 3, the rate-independent nominal stress in a uniaxial compression experiment at the equilibrium state can be determined

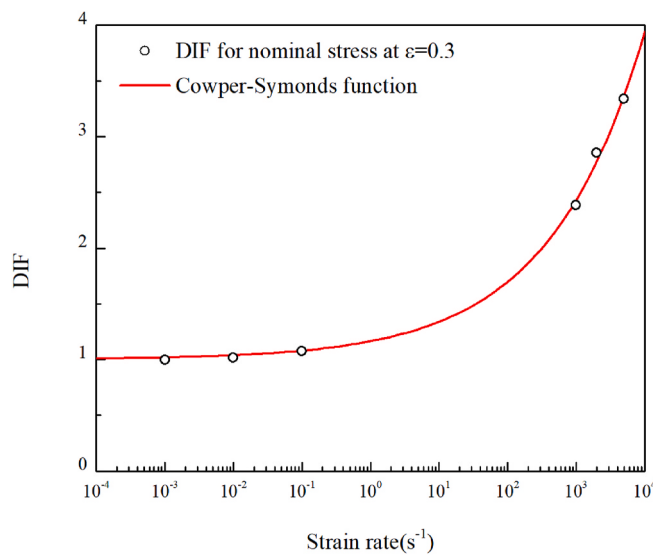


**Fig. 9.** DIF for nominal stress at nominal strain 0.3 and proposed Cowper-Symonds function.

using Eq. (44). The nominal stress is expressed Eq. (44) shows the correlation between the nominal strain and nominal stress in a state of equilibrium. As shown in Fig. 10, the reference curve for the identification of these three parameters was selected based on the uniaxial compressive test results at a strain rate of  $0.001\text{ s}^{-1}$ . The maximum duration of loading conducted in the quasi-static experiment was 600 s at the strain rate of  $0.001\text{ s}^{-1}$ . This extended period is considered relatively long in terms of enabling the sample to reach the equilibrium state. The parameters identified with the least squares method for the hyperelastic energy function, were presented in Table 1.

### 5.3. Results of DMA tests

During the dynamic temperature sweep test, the complex dynamic moduli were obtained at a frequency of 1 Hz. The influence of temperature on the storage and loss moduli, as well as the corresponding loss tangent ( $\tan \delta$ ), is presented in Fig. 11.

Three distinct regions were observed for the storage modulus. First, the glassy zone exhibited a slight decrease in modulus with increasing temperature. Second, the transition region displayed a significant change in modulus over several decades. Finally, the rubbery region or

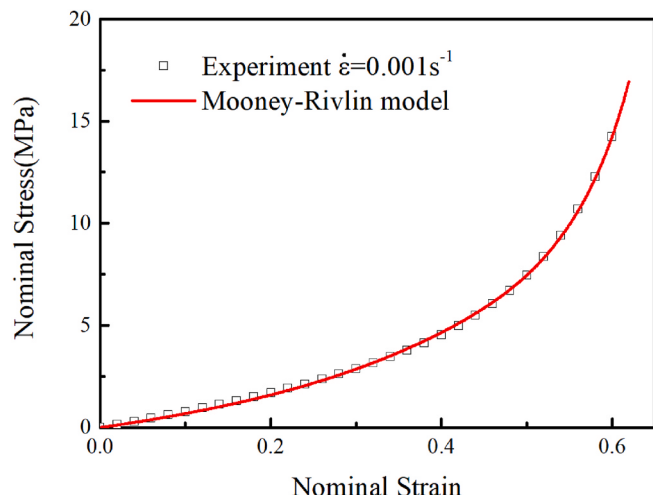


**Fig. 10.** Result of the uniaxial compressive test obtained at a reference strain rate of  $0.001\text{ s}^{-1}$ .

**Table 1**

Parameters of the hyperelastic function identified with the least squares method.

$\bar{A}_{01}$ (MPa)	$\bar{A}_{10}$ (MPa)	$\bar{A}_{11}$ (MPa)	$R^2$
1.7549	-0.5341	0.0844	0.99

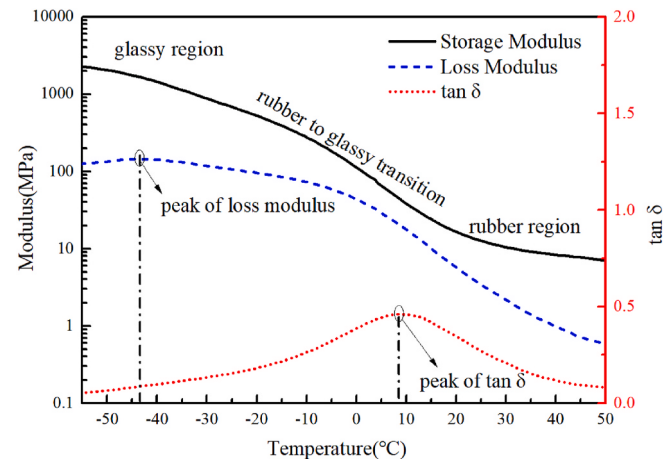


**Fig. 11.** Results of the temperature sweep test for the polyurethane sample.

plateau zone exhibited only a slight decrease in modulus with temperature. At the peak point of loss modulus in the experiment, the temperature reached  $-44^\circ\text{C}$ , signifying the beginning of the transition from a glassy to a rubbery state. At the maximum point of  $\tan \delta$ , the temperature recorded was  $8^\circ\text{C}$ , indicating the peak of the loss factor. The temperature range utilised in the temperature sweep test spanned from  $-55$  to  $50^\circ\text{C}$ , encompassing the glass transition temperature and a significant portion of the transition region between the glassy and rubbery states.

As presented in Fig. 12, the storage modulus was recorded at a series of frequencies for each temperature increment. The application of the TTSP enables the shifting of experimentally determined material curves, resulting in the creation of a continuous curve that spans a wide range of frequencies.

In the process of constructing the master curve, the storage modulus was horizontally shifted to attain a continuous S-shaped curve. The horizontal shift factors, also known as time-temperature shift factors, were determined using the TTSP. The shift factors were evaluated using a nonlinear minimization algorithm program, which is based on the

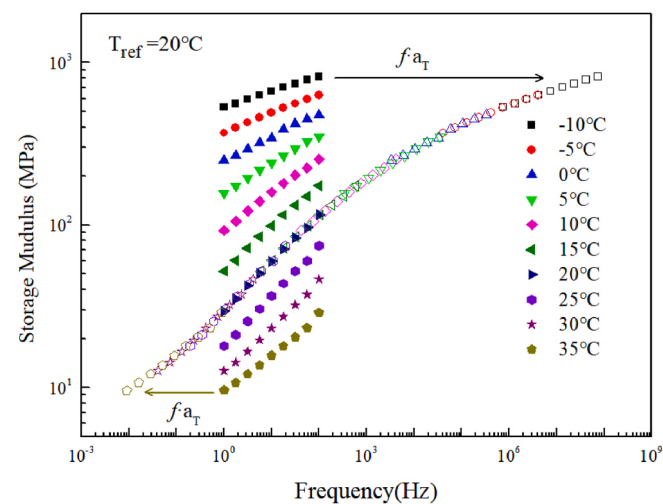


**Fig. 12.** Multi-frequency test results and construction of the master curve.

standard method outlined in ISO18437-6 [62]. This program enabled us to determine a dynamic modulus master curve by shifting the individual curve at each temperature. The reduced frequency, denoted as  $f_R$ , was then calculated using the equation  $f_R = a_T \times f$ , where  $a_T$  represents the shift factor, and  $f$  represents the loading frequency in Hz. The reference temperature, which corresponds to the unshifted dataset, was recorded as 20 °C. The shift factor can be characterized by the widely used Williams–Landel–Ferry (WLF) equation, expressed as follows [63]:

$$\log_{10} a_T = -\frac{C_1(T - T_{ref})}{C_2 + (T - T_{ref})} \quad (58)$$

The parameters in the WLF equation, namely  $C_1 = 16.5$  and  $C_2 = 113.6$  °C, were determined through fitting the shift factors in Fig. 13.

#### 5.4. Determination of parameters for viscoelastic behaviour with continuous relaxation spectrum

##### 5.4.1. Establishing the continuous relaxation spectrum function

Previous studies have highlighted the significance of a continuous relaxation spectrum, which has been utilised to analyse the dynamic modulus test data, resulting in the determination of positive Prony series parameters and the generation of a well-fitted curve for the relaxation modulus.

The continuous relaxation spectrum  $H(\tau)$  can be defined as a function of the relaxation time  $\tau$  in both the time and frequency domains. This paper introduces a straightforward and effective method for directly obtaining continuous relaxation spectra of polyurethane elastomers from complex (dynamic) modulus test data, specifically under uniaxial loading conditions. With this method, continuous spectra are derived directly from the frequency-domain master curves derived from the experimental data.

First, the data for the complex (dynamic) modulus test under uniaxial loading conditions are calculated using a multi-frequency test, as outlined in Section 3.3. The master curve can be constructed by applying the time–temperature superposition principle to the modulus data obtained at various frequencies and temperatures. The generalised sigmoidal model in Eq. (50) is used to accurately fit the master curve. These parameters were determined using MATLAB, specifically the *lsqcurvefit* function. As shown in Fig. 14, the master curve can be accurately fitted to a sigmoid function in Eq. (50). The optimal model parameters obtained using the least squares method are listed in Table 2.

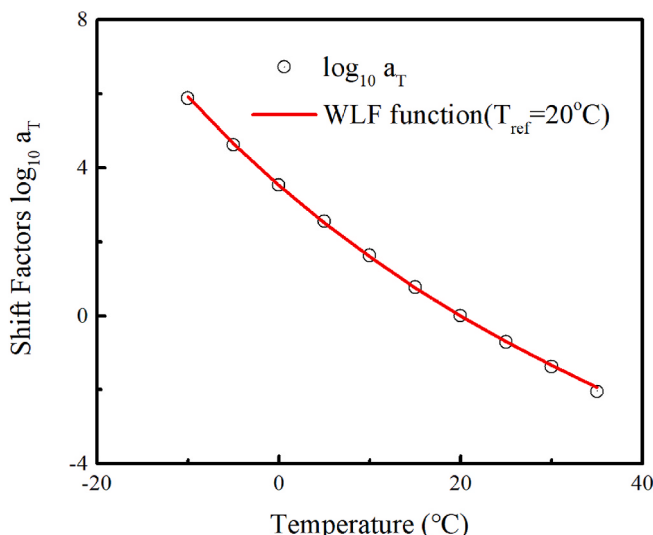


Fig. 13. Shift factors and curve of the WLF function.

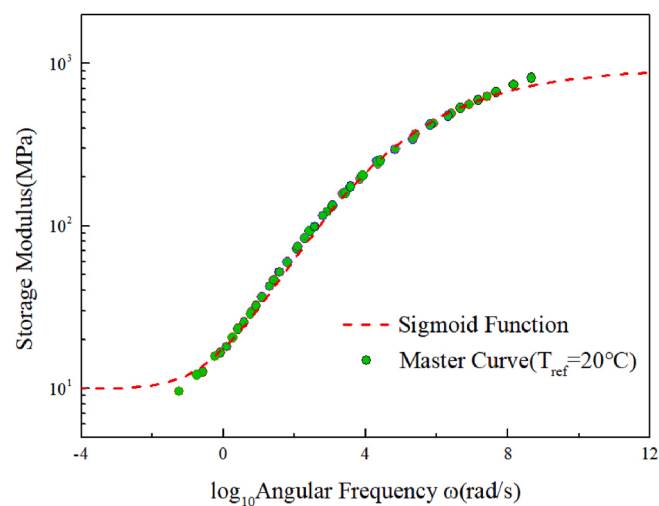


Fig. 14. Master curve that has been fitted with a sigmoid function.

Table 2  
Optimal model parameters of sigmoid function.

$\alpha_s$	$\beta_s$	$\gamma_s$	$\delta_s$	$R^2$
1.9712	1.3548	-0.4149	1	0.9914

##### 5.4.2. Development of the prony series model

The time-dependent relaxation function, which follows the Prony series, is estimated using a continuous relaxation spectrum. As mentioned in Section 2, the Prony series can be used to model  $g(t)$  and determine the viscoelastic parameters based on continuous relaxation spectrum of the material using Eqs. (51) and (52).

By understanding the fundamental meaning of the relaxation spectrum, a continuous distribution of relaxation times in the Prony series or the time-dependent relaxation function can be determined through Eq. (9). A general form of Eq. (9) is expressed as:

$$E(t) \cong E_\infty + \sum_{i=1}^N (H(\tau_i) \times \Delta \ln \tau_i) \exp(-t / \tau_i) \quad (59)$$

The relaxation time was converted in terms of the base-10 logarithmic scale typically in common usage. This conversion involved representing the distance  $\Delta \ln \tau_i$  between two near relaxation time  $\tau_{i+1}$  and  $\tau_i$  in terms of  $\Delta \lg \tau_i = \Delta \ln \tau_i / \ln 10$  on an axis using the base-10 logarithmic scale. For convenience, the values of  $\tau_i$  were predetermined and evenly spaced on a logarithmic axis with a base of 10. Hence, the distribution of relaxation times was logarithmically spaced within each decade of the timescale. The interval distance was defined as the number of sub-domains, denoted as  $1 / \Delta \lg \tau_i$ . Studies have demonstrated that the master curves generated by the Prony series models provide a good fit to the test data when the interval points are spaced within each decade [53].

The effective range for relaxation behaviour is determined by the time scale of measurements. Knauss et al. [34] discussed this problem and stated that the effective range was typically determined by the resolution of the timing equipment or the dynamic response of the test frame at the short-time end, and by environmental stability of the device at long-time end. The lower limit of the range is determined by data acquisition sampling of SHPB tests. In our work, it is enough by selecting  $10^{-7}$  s. The upper limit is determined by the loading duration of the quasi-static experiment, and herein 100 s is chosen, which is suitable for the relaxation behaviour required for quasi-static loading experiments. Therefore, the effective range of the relaxation time is determined to be from  $10^{-7}$  s– $10^2$  s.

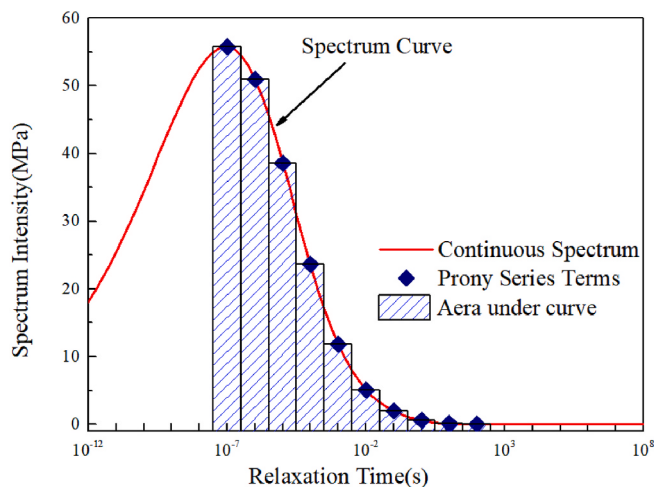


**Fig. 15.** Determination of parameters for viscoelastic behaviour with a continuous relaxation spectrum.

The continuous relaxation modulus was calculated using Eq. (52). As shown in Fig. 15, a schematic overview of the procedure was employed for parameter identification using a continuous relaxation spectrum. The continuous spectrum function in Eq. (52) is represented by a red line. The blue squares represent the designated relaxation times and spectral intensities. The area of region between a near distance of  $\Delta \ln \tau_i$  and under the continuous relaxation spectrum curve is referred to as the relaxation modulus. Specifically, the long-term modulus is determined by the minimum value of the master curve,  $E_\infty = 10^{8\text{s}}$ . The relative parameters of modulus were determined according to the process of normalisation, and the long-term parameter  $g_\infty$  was determined using the restrictions outlined in Eq. (7). A set of viscoelastic parameters ( $N = 10$ ) was ultimately determined to accurately represent the viscoelastic behaviour across a wide range of timescales, as presented in Table 3.

### 5.5. Numerical validation of the proposed hyper-viscoelastic model

The proposed hyper-viscoelastic constitutive model consists of two sets of parameter variables that are determined independently. When the parameter identification process is completed, the model can be utilised to accurately depict and predict the stress-strain correlation in the uniaxial compressive behaviour of the polyurethane material. The next section describes the validation of the proposed hyper-viscoelastic model through a comparative study between the numerical predictions obtained from the hyper-viscoelastic model and the experimental results of the uniaxial compressive behaviour under quasi-static and high strain rates.

The constitutive model proposed in Eqs. (43) and (46) was utilised to analyse the responses of polyurethane at six different strain rates, which have been observed to exhibit rate dependence in previous studies. To

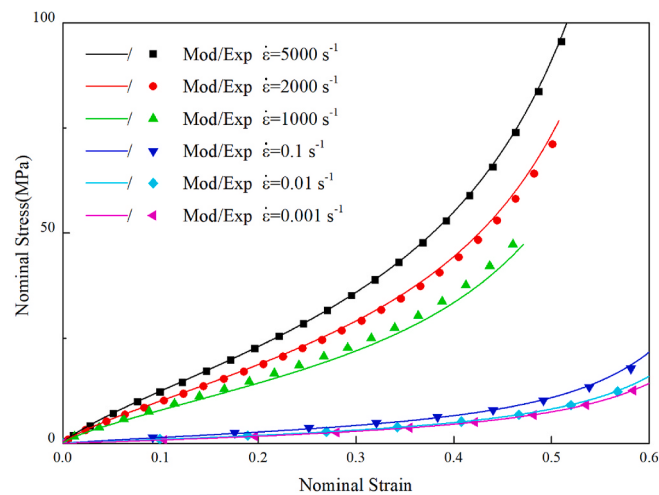


**Fig. 16.** Comparison of hyper-viscoelastic model and experimental data.

assess the accuracy and further validate the proposed constitutive model, we compared the experimental and numerical results of the nominal stress-strain curves of polyurethane. This comparison was conducted under quasi-static conditions and high-rate conditions, as shown in Fig. 16. The materials that underwent low- and high-strain-rate compression exhibited significant concurrence between the proposed model and experimental data, suggesting the capability of the model to accurately depict the dynamic characteristics of elastomeric materials across various strain rates. Although disparities were observed in the nominal stress-strain curves between the experimental results and the constitutive models for both the quasi-static compressive tests and high-rate tests, the relative error percentages remained within acceptable limits.

Though only compression properties of elastomer are analyzed to build the model proposed in this work, the constitutive framework is allowable for representing material behavior under different modes, such as tensile or shear deformation. Deformation gradient tensors between tensile and compressive modes are nearly similar in the constitutive framework. Thus, the stress response of tensile and compressive loading can be obtained using the same formulation in the proposed model. It is able to capture the nonlinear, rate-dependent phenomena of elastomeric materials for tension mode [6,7], with supplementation of their viscoelastic properties. As a similar hyper-viscoelastic model was successfully developed by Tayeb [45], by using the method of comparing finite element simulation result with a semi-analytical solution for shear deformation, the proposed model could be further extended for capturing shear behavior with the aid of an additional shear experimental results.

### 6. Conclusion

This study presents a hyper-viscoelastic model that effectively characterizes the mechanical behaviour of polyurethane elastomers over a wide range of strain rates ( $0.001\text{--}5000\text{ s}^{-1}$ ). The proposed model combines the internal variables method with a modified generalised Maxwell viscoelastic model to capture rate-dependent effects at large strain. The viscoelastic properties were determined using a methodology that applies the time-temperature superposition principle and a continuous relaxation spectrum. The method described in our work enables the conversion of frequency-domain properties into time-domain relaxation properties, allowing for the systematic assessment of dynamic analysis across a wide range of timescales or frequency scales. This approach leads to a thorough evaluation for developing a relaxation modulus model with positive relaxation moduli and effective relaxation times distributed across a wide range of time scales.

**Table 3**  
Model parameters determined using a continuous relaxation spectrum approach.

N	$\Delta \lg \tau_i$	$\tau_i(\text{s})$	$H(\tau_i)$	$g_i$	$g_\infty$
10	1	$10^{-7}$	55.7535	0.2874	0.0225
		$10^{-6}$	50.9658	0.2671	
		$10^{-5}$	38.5954	0.2064	
		$10^{-4}$	23.6501	0.1292	
		$10^{-3}$	11.8669	0.0660	
		$10^{-2}$	5.1152	0.0288	
		$10^{-1}$	1.9363	0.0111	
		$10^0$	0.5606	0.0033	
		$10^1$	0.0802	$5.296 \times 10^{-4}$	
		$10^2$	0.0021	$1.795 \times 10^{-5}$	

Furthermore, we provide new insights into modelling relaxation behaviour, which is essential for studying the mechanical response at high strain rates, especially in impact absorption. Further investigations will be performed to expand the model to various polymer materials and other modes of deformation. The proposed methodology in this work is expected to be integrated as a constitutive material model into a general finite element code. This integration will facilitate the evaluation and development of protective structures under intense dynamic loading conditions.

#### CRediT authorship contribution statement

**Penghao Pei:** Formal analysis, Investigation, Methodology, Software, Writing – original draft. **Yueming Du:** Investigation, Writing – review & editing. **Yinggang Miao:** Validation, Writing – review & editing. **Tao Suo:** Conceptualization, Funding acquisition, Supervision.

#### Declaration of competing interest

The authors declare that they have no known competing financial interests or personal relationships that could have appeared to influence the work reported in this paper.

#### Data availability

Data will be made available on request.

#### Acknowledgements

This work was supported by the National Natural Science Foundations of China (Grant Nos. 12025205, 12141203, 12172304) and the Key Research and Development Plan of Shaanxi Province (No. 2023-GHZD-12).

#### References

- [1] D. Pacek, J. Rutkowski, The composite structure for human body impact protection, *Compos. Struct.* 265 (2021).
- [2] A. Rühl, S. Kolling, J. Schneider, Characterization and modeling of poly(methyl methacrylate) and thermoplastic polyurethane for the application in laminated setups, *Mech. Mater.* 113 (2017) 102–111.
- [3] H.M.C.C. Somaratna, S.N. Raman, D. Mohotti, et al., The use of polyurethane for structural and infrastructural engineering applications: a state-of-the-art review, *Construct. Build. Mater.* 190 (2018) 995–1014.
- [4] B. Cheng, W. Gao, X. Ren, et al., A review of microphase separation of polyurethane: characterization and applications, *Polym. Test.* 107 (2022) 107489.
- [5] H.J. Qi, M.C. Boyce, Stress-strain behavior of thermoplastic polyurethanes, *Mech. Mater.* 37 (2005) 817–839.
- [6] Y. Miao, H. He, Z. Li, Strain hardening behaviors and mechanisms of polyurethane under various strain rate loading, *Polym. Eng. Sci.* 60 (2020) 1083–1092.
- [7] Y. Miao, H. Zhang, H. He, et al., Mechanical behaviors and equivalent configuration of a polyurea under wide strain rate range, *Compos. Struct.* 222 (2019).
- [8] J. Yi, M.C. Boyce, G.F. Lee, et al., Large deformation rate-dependent stress-strain behavior of polyurea and polyurethanes, *Polymer* 47 (2006) 319–329.
- [9] S.S. Sarva, S. Deschanel, M.C. Boyce, et al., Stress-strain behavior of a polyurea and a polyurethane from low to high strain rates, *Polymer* 48 (2007) 2208–2213.
- [10] Z. Liao, X. Yao, L. Zhang, et al., Temperature and strain rate dependent large tensile deformation and tensile failure behavior of transparent polyurethane at intermediate strain rates, *Int. J. Impact Eng.* 129 (2019) 152–167.
- [11] J.T. Fan, J. Weerheim, L.J. Sluys, Dynamic compressive mechanical response of a soft polymer material, *Mater. Des.* 79 (2015) 73–85.
- [12] H. Cho, S. Mayer, E. Pösel, et al., Deformation mechanisms of thermoplastic elastomers: stress-strain behavior and constitutive modeling, *Polymer* 128 (2017) 87–99.
- [13] H.M.C.C. Somaratna, S.N. Raman, D. Mohotti, et al., Hyper-viscoelastic constitutive models for predicting the material behavior of polyurethane under varying strain rates and uniaxial tensile loading, *Construct. Build. Mater.* (2020) 236.
- [14] M. Jahanmardi, H. Hosseini-Toudeshky, M.S. Goodarzi, et al., Modified hyper-viscoelastic damage evolution constitutive model for polyurethane materials – an experimental and numerical investigation, *Mech. Adv. Mater. Struct.* (2023) 1–12.
- [15] W. Findley, J. Lai, K. Onaran, et al., Creep and Relaxation of Nonlinear Viscoelastic Materials with an Introduction to Linear Viscoelasticity, 1977.
- [16] L.M. Yang, V.P.W. Shim, C.T. Lim, A visco-hyperelastic approach to modelling the constitutive behaviour of rubber, *Int. J. Impact Eng.* 24 (2000) 545–560.
- [17] M.S.H. Fatt, X. Ouyang, Integral-based constitutive equation for rubber at high strain rates, *Int. J. Solid Struct.* 44 (2007) 6491–6506.
- [18] J. Shim, D. Mohr, Rate dependent finite strain constitutive model of polyurea, *Int. J. Plast.* 27 (2011) 868–886.
- [19] C.M. Roland, Mechanical behavior of rubber at high strain rates, *Rubber Chem. Technol.* 79 (2006) 429–459.
- [20] R.B. Bogoslovov, C.M. Roland, R.M. Gamache, Impact-induced glass transition in elastomeric coatings, *Appl. Phys. Lett.* 90 (2007).
- [21] J. Liu, G. Gorbacheva, H. Lu, et al., A dynamic hysteresis model for customized glass transition in amorphous polymer towards multiple shape memory effects, *Smart Mater. Struct.* (2022) 31.
- [22] J. Liu, H. Lu, Y.-Q. Fu, Spinodal dynamics of metastable glass transition domains in amorphous polymer towards thermomechanically tailororable shape memory effect, *Sci. China Technol. Sci.* 66 (2023) 2432–2440.
- [23] A.V. Amirkhizi, J. Isaacs, J. Mcgee, et al., An experimentally-based viscoelastic constitutive model for polyurea, including pressure and temperature effects, *Philos. Mag. A* 86 (2006) 5847–5866.
- [24] R.J. Clifton, X. Wang, T. Jiao, A physically-based, quasilinear viscoelasticity model for the dynamic response of polyurea, *J. Mech. Phys. Solid.* 93 (2016) 8–15.
- [25] J. Bonet, Large strain viscoelastic constitutive models, *Int. J. Solid Struct.* 38 (2001) 2953–2968.
- [26] J.C. Simo, On a fully three-dimensional finite-strain viscoelastic damage model: formulation and computational aspects, *Comput. Methods Appl. Mech. Eng.* 60 (1987) 153–173.
- [27] G.A. Holzapfel, On large strain viscoelasticity: continuum formulation and finite element applications to elastomeric structures, *Int. J. Numer. Methods Eng.* 39 (1996) 3903–3926.
- [28] A. Tayeb, M. Arfaoui, A. Zine, et al., On the nonlinear viscoelastic behavior of rubber-like materials: constitutive description and identification, *Int. J. Mech. Sci.* 130 (2017) 437–447.
- [29] P. Haupt, A. Lion, On finite linear viscoelasticity of incompressible isotropic materials, *Acta Mech.* 159 (2002) 87–124.
- [30] S. Reese, S. Govindjee, A theory of finite viscoelasticity and numerical aspects, *Int. J. Solid Struct.* 35 (1998) 3455–3482.
- [31] D. Chen, H. Wu, J.S. Wei, et al., Nonlinear visco-hyperelastic tensile constitutive model of spray polyurea within wide strain-rate range, *Int. J. Impact Eng.* 163 (2022) 104184.
- [32] S.M. Goh, M.N. Charalambides, J.G. Williams, Determination of the constitutive constants of non-linear viscoelastic materials, *Mech. Time-Dependent Mater.* 8 (2004) 255–268.
- [33] A.F.M.S. Amin, A. Lion, S. Sekita, et al., Nonlinear dependence of viscosity in modeling the rate-dependent response of natural and high damping rubbers in compression and shear: experimental identification and numerical verification, *Int. J. Plast.* 22 (2006) 1610–1657.
- [34] W.G. Knauss, J. Zhao, Improved relaxation time coverage in ramp-strain histories, *Mech. Time-Dependent Mater.* 11 (2007) 199–216.
- [35] Z.Z. Jia, A.V. Amirkhizi, W. Nantasetphong, et al., Experimentally-based relaxation modulus of polyurea and its composites, *Mech. Time-Dependent Mater.* 20 (2016) 155–174.
- [36] M. Esposito, L. Sorrentino, P. Krejci, et al., Modelling of a visco-hyperelastic polymeric foam with a continuous to discrete relaxation spectrum approach, *J. Mech. Phys. Solid.* 142 (2020).
- [37] D. Ionita, M. Cristea, C. Gaina, Prediction of polyurethane behaviour via time-temperature superposition: meanings and limitations, *Polym. Test.* 83 (2020).
- [38] T. Hána, T. Janda, J. Schmidt, et al., Experimental and numerical study of viscoelastic properties of polymeric interlayers used for laminated glass: determination of material parameters, *Materials* 12 (2019) 2241.
- [39] B. Eva, P. Fernández, N. Álvaro, et al., Optimal discrete-time Prony series fitting method for viscoelastic materials, *Mech. Time-Dependent Mater.* 23 (2018) 193–206.
- [40] I. Emri, N.W. Tschoegl, Generating line spectra from experimental responses. Part IV: application to experimental data, *Rheol. Acta* 33 (1994) 60–70.
- [41] J.D. Ferry, Viscoelastic Properties of Polymers, third ed., 1980.
- [42] N.W. Tschoegl, The Phenomenological Theory of Linear Viscoelastic Behavior, 1989.
- [43] B.D. Coleman, M.E. Gurtin, Thermodynamics with internal state variables, *J. Chem. Phys.* 47 (1967) 597. &
- [44] K. Naroei, M. Arman, Generalization of exponential based hyperelastic to hyper-viscoelastic model for investigation of mechanical behavior of rate dependent materials, *J. Mech. Behav. Biomed. Mater.* 79 (2018) 104–113.
- [45] A. Tayeb, M. Arfaoui, A. Zine, et al., Investigation of the nonlinear hyper-viscoelastic behavior of elastomers at finite strain: implementation and numerical validation, *The European Physical Journal Plus* 137 (2022).
- [46] H. Pouriyaveali, Y.B. Guo, V.P.W. Shim, A constitutive description of elastomer behaviour at high strain rates – a strain-dependent relaxation time approach, *Int. J. Impact Eng.* 47 (2012) 71–78.
- [47] V. Dorléans, R. Delille, D. Notta-Cuvier, et al., Time-temperature superposition in viscoelasticity and viscoplasticity for thermoplastics, *Polym. Test.* 101 (2021) 107287.
- [48] M. Müller-Pabel, J.A. Rodríguez Agudo, M. Gude, Measuring and understanding cure-dependent viscoelastic properties of epoxy resin: a review, *Polym. Test.* 114 (2022) 107701.

- [49] S. Bhattacharjee, A.K. Swamy, J.S. Daniel, Continuous relaxation and retardation spectrum method for viscoelastic characterization of asphalt concrete, *Mech. Time-Dependent Mater.* 16 (2011) 287–305.
- [50] H. Lv, H. Liu, Y. Tan, et al., Improved methodology for identifying Prony series coefficients based on continuous relaxation spectrum method, *Mater. Struct.* (2019) 52.
- [51] I. Emri, B.S. von Bernstorff, R. Cvelbar, et al., Re-examination of the approximate methods for interconversion between frequency- and time-dependent material functions, *J Non-Newton Fluid* 129 (2005) 75–84.
- [52] K.S. Cho, Viscoelastic Spectrum, *Viscoelasticity of Polymers: Theory and Numerical Algorithms*, Springer Netherlands, Dordrecht, 2016, pp. 397–435.
- [53] R. Luo, H.J. Lv, H.Q. Liu, Development of Prony series models based on continuous relaxation spectrums for relaxation moduli determined using creep tests, *Construct. Build. Mater.* 168 (2018) 758–770.
- [54] G.T. Gray III, W.R. Blumenthal, *Split-Hopkinson Pressure Bar Testing of Soft Materials. Mechanical Testing and Evaluation*, ASM International, 2000, pp. 488–496.
- [55] C.R. Sivior, J.L. Jordan, High strain rate mechanics of polymers: a review, *Journal of Dynamic Behavior of Materials* 2 (2016) 15–32.
- [56] H. Guo, W.G. Guo, A.V. Amirkhizi, et al., Experimental investigation and modeling of mechanical behaviors of polyurea over wide ranges of strain rates and temperatures, *Polym. Test.* 35 (2016) 234–244.
- [57] W. Chen, B. Zhang, M.J. Forrestal, A split Hopkinson bar technique for low-impedance materials, *Exp. Mech.* 39 (1999) 81–85.
- [58] H. Zhao, G. Gary, J.R. Klepaczko, On the use of a viscoelastic split hopkinson pressure bar, *Int. J. Impact Eng.* 19 (1997) 319–330.
- [59] T.P.M. Johnson, S.S. Sarva, S. Socrate, Comparison of low impedance split-hopkinson pressure bar techniques in the characterization of polyurea, *Exp. Mech.* 50 (2010) 931–940.
- [60] Y. Miao, Y. Wang, W. Du, et al., Theoretical instructions for experimenting controllable Hopkinson pressure bar, *Polym. Test.* 108 (2022).
- [61] H. Chen, L.R. Hart, W. Hayes, et al., Mechanical characterisation and modelling of a thermoreversible superamolecular polyurethane over a wide range of rates, *Polymer* 221 (2021) 123607.
- [62] ISO18437-6, *Mechanical Vibration and Shock — Characterization of the Dynamic Mechanical Properties of Visco-Elastic Materials — Part 6: Time-Temperature Superposition*, International Organization for Standardization, 2017.
- [63] M.L. Williams, R.F. Landel, J.D. Ferry, The temperature dependence of relaxation mechanisms in amorphous polymers and other glass-forming liquids, *J. Am. Chem. Soc.* 77 (1955) 3701–3707.